

University of Nebraska - Lincoln
DigitalCommons@University of Nebraska - Lincoln

Civil Engineering Faculty Publications

Civil Engineering


1-2014

Equipment Fragility Due to Shock Response

Christopher Y. Tuan

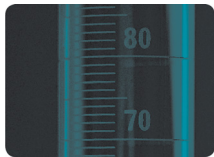
University of Nebraska-Lincoln, ctuan1@unl.edu

Follow this and additional works at: <http://digitalcommons.unl.edu/civilengfacpub>

 Part of the [Engineering Science and Materials Commons](#), [Other Engineering Commons](#), [Risk Analysis Commons](#), and the [Structural Engineering Commons](#)

Tuan, Christopher Y., "Equipment Fragility Due to Shock Response" (2014). *Civil Engineering Faculty Publications*. 71.
<http://digitalcommons.unl.edu/civilengfacpub/71>

This Article is brought to you for free and open access by the Civil Engineering at DigitalCommons@University of Nebraska - Lincoln. It has been accepted for inclusion in Civil Engineering Faculty Publications by an authorized administrator of DigitalCommons@University of Nebraska - Lincoln.



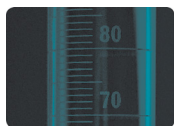
Journal of Testing and Evaluation

Christopher Y. Tuan

DOI: 10.1520/JTE20130018

Equipment Fragility Due to Shock Response

VOL. 42 / NO. 1 / JANUARY 2014



Manuscript received January 20, 2013; accepted for publication May 16, 2013; published online August 23, 2013.

Professor, Dept. of Civil Engineering, Univ. of Nebraska-Lincoln, Peter Kiewit Institute, 1110 S. 67th St., Omaha, NE 68182-0178, United States of America, e-mail: ctuan1@unl.edu

Christopher Y. Tuan

Equipment Fragility Due to Shock Response

Reference

Tuan, Christopher Y., "Equipment Fragility Due to Shock Response," *Journal of Testing and Evaluation*, Vol. 42, No. 1, 2014, pp. 1-11, doi:10.1520/JTE20130018. ISSN 0090-3973

ABSTRACT

Because of its simplicity, the shock response spectrum has become widely used as a means of describing the shock responses and fragilities of structures and equipment. This paper focuses on the drawbacks of using the shock response spectrum for defining equipment shock tolerance. A cantilever beam with a tip mass was used to model a hypothetical piece of equipment subjected to strong ground motion such as that caused by an explosion. The exact solution from a detailed modal analysis shows that multiple modes of response were excited. Contributions from higher modes can be more predominant than that from the fundamental mode. Assuming the total response of equipment is predominantly in the first mode can lead to significant error. Current shock spectrum procedures for equipment fragility assessment are inadequate, not only because of the physical limitations of shake table tests, but also because of the lack of a reliable analytical model.

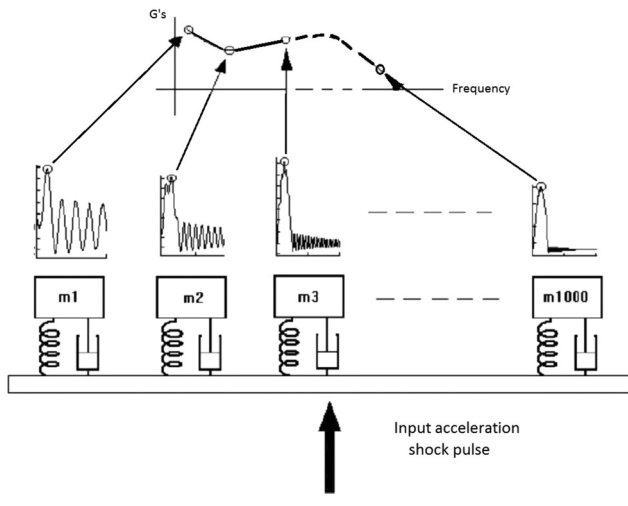
Keywords

equipment, fragility, shock response spectrum, modal analysis, spectral analysis, fast Fourier transform

Introduction

A shock response spectrum (SRS) is the envelope of the maximum response amplitudes of an ensemble of damped single-degree-of-freedom (SDOF) oscillators subjected to a specified support excitation over a frequency range. The construction of an SRS is depicted in **Fig. 1**. Because of its simplicity, SRS has become widely employed as a means of describing the shock responses and fragilities of structures [1-9] and equipment [10-15].

This paper focuses on the drawbacks of using SRS for defining equipment shock tolerance. Several papers have already pointed out the shortcomings of using a design response spectrum, such as multi-dimensional motion and the combinatorial methodologies for the inclusion of

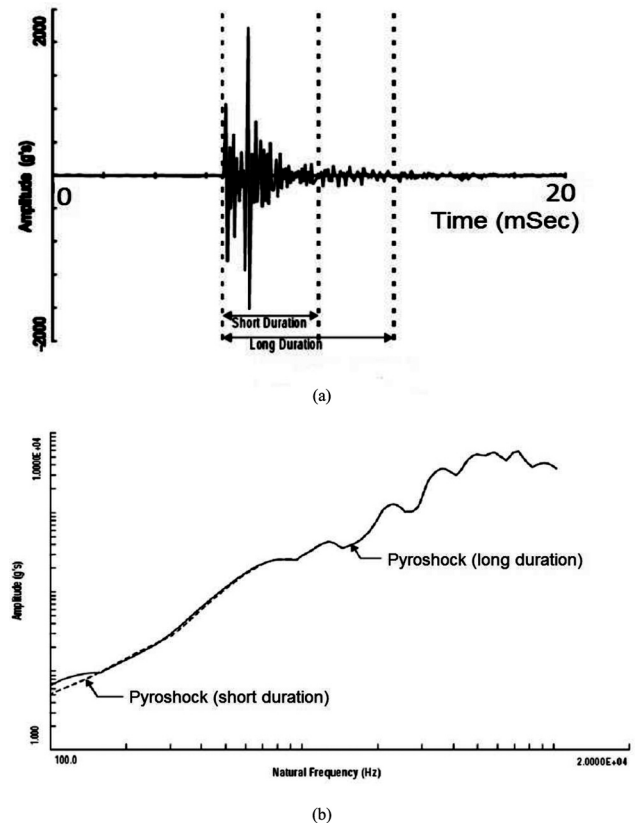
FIG. 1 Shock response spectrum (SRS).

higher modes [16,17] and nonlinear responses [18]. This paper illustrates that strong ground motion of short duration, such as that caused by an explosion, will excite multiple vibrational modes in equipment. Assuming that the total response of the equipment is predominantly in the first mode can lead to significant error. Current shock spectrum procedures for equipment fragility assessment are inadequate, not only because of the physical limitations of shake table tests, but also because of the lack of a reliable analytical model.

Equipment Fragility

Electronic equipment and system components are routinely subjected to shock and vibration testing in order to identify design flaws and functional weaknesses. Sometimes the tests are also conducted in extreme temperature environments. Response spectra based on known earthquake accelerograms or specified vibration time-histories are useful for dynamic characterizations such as resonance, damping, fatigue endurance, etc. Shock testing, in contrast, involves a high magnitude of stress, acceleration, or displacement for a short duration. The waveforms of shock pulses are commonly specified as half-sine or sawtooth. Many shock test specifications exist, including military (MIL-STD-202G [19]), regulatory (ISO 16750-3 [20]), and automotive industry standards (SAE J1455 [21]), as well as those provided by the equipment manufacturers. The waveform, peak acceleration, duration, and initial velocity change of the shock pulses are specified in these standards.

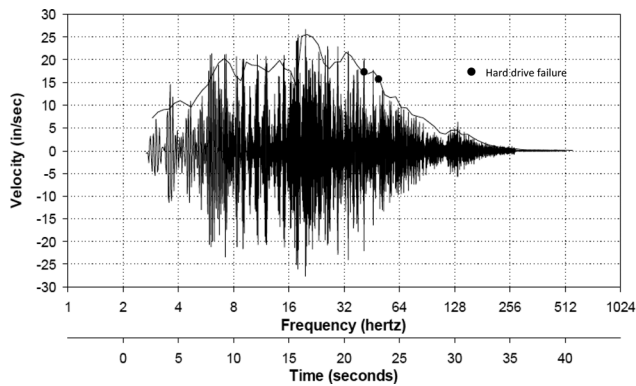
A fragility spectrum displays equipment's capacity to resist transient support motion in terms of motion amplitude versus frequency. Therefore, it is essentially an envelope of response spectra at which equipment failure occurs. Equipment failure is usually defined as mechanical damage or loss of function, including intermittent electrical contacts, touching and shorting

FIG. 2 (a) Pyrotechnic shock accelerogram. (b) SRS of the pyroshocks [22].

of electrical parts, seal damage, optical misalignment, cracking and rupturing in components, structural deformation, and failure. A typical accelerogram resulting from an explosion [22], known as "pyrotechnic shock" or "pyroshock," is shown in Fig. 2(a), and its associated SRS shown in Fig. 2(b). In general, damage due to short-duration pulses is a function of the initial velocity change, whereas that due to long-duration pulses is a function of the peak acceleration and waveform. Method 516.6 in the military standard MIL-STD-810G [23] provides detailed descriptions of fragility test and shock evaluation procedures. Expressing equipment fragility in terms of SRSs greatly simplifies the design of equipment shock isolation. However, the applicability of a design shock spectrum is often questionable.

The approach commonly employed to determine equipment fragility is to physically test a piece of equipment on a shake table with a certain intensity and frequency. Failure modes of equipment may be related to amplitudes and frequencies of the motions at various locations on the equipment. An "Equipment Fragility and Protection Procedure" was developed by Wilcoski et al. [11] to determine whether equipment is vulnerable to prescribed support motions. The purpose of the procedure is to determine the levels of motion at which equipment fails across a broad frequency range.

FIG. 3 Shaker table vertical motion time history with desktop computer failure data [11].

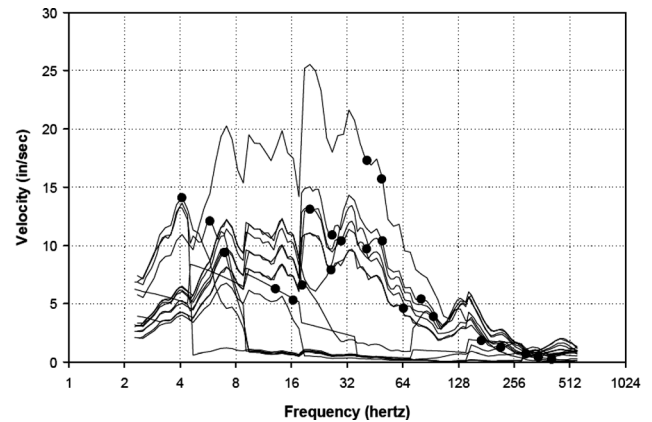


During the development of the procedure, fragility data were gathered based on shake table tests. In these tests, a random signal is passed through high- and low-pass filters to drive the shake table. This process creates a random motion, with the energy of the motion concentrated within a narrow frequency band, and the center frequency moves at a given sweep rate (e.g., the center frequency is doubled every 5 s). The intensity of the base motion is progressively increased until failure occurs. The frequency range of the shake table motion is physically limited to about 3000 Hz. Fortunately, equipment is vulnerable to low-frequency amplitudes and is unlikely to fail at very high frequencies. For instance, a desktop computer was subjected to a series of shake table tests in the vertical direction [11]. The time-history of support motion in a typical test and the failure data are shown in Fig. 3. The fragility data collected from all the tests are presented in Fig. 4 in terms of the support spectral velocity amplitudes. The resulting plot is also known as the “fragility spectrum.” A fragility spectrum may be used to develop methods of protecting equipment, through either strengthening or isolation of the equipment. However, for shock-induced base motion, equipment modal responses associated with higher modes might be significant, as is illustrated in an example later in this paper.

Limitations of the Shock Spectrum Approach

The use of SRSs for equipment fragility assessment is oversimplified and has several inherent sources of error. The most important source of error is that an SRS does not correspond to a unique input time-history. An infinite number of different base motions can generate a given SRS. These different base motions could vary greatly in duration, frequency content, and amplitude. The main assumption behind the SRS approach to equipment fragility is that equipment failure is independent of the input waveform. All input base motions corresponding to the

FIG. 4 Fragility spectrum of the desktop computer [11].



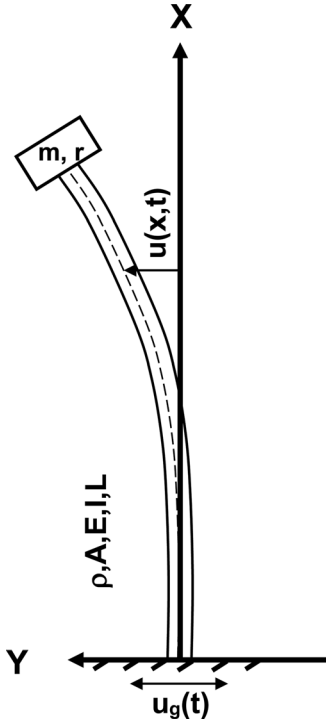
SRS are assumed to result in the same failure mode. The possibility of a single item of equipment possessing multiple failure modes is generally not considered. In reality, equipment fragility spectra are valid only for frequencies close to the natural frequencies at which the equipment was actually tested. Extrapolating equipment fragility based on existing databases of, for example, shipboard testing data [24] to the shock environment resulting from an explosion is questionable but routinely done. The validity of this extrapolation has not been verified. Equipment qualification methods are often based on either response spectra or the power spectral density of support accelerations, which does not provide information on the specific frequency of motion that caused failure. Further, a base motion is generally three-dimensional, and the peak response amplitude might be quite different from that of unidirectional base motion.

Years of earthquake engineering research have shown that all earthquake response spectra display similar characteristics. Approximate upper bound response spectra may be constructed based only on the peak displacement, velocity, and acceleration of the oscillator base. Kiger et al. [25] have shown that in-structure SRSs can be bounded by multiplying the peak in-structure displacement, velocity, and acceleration by factors of 1.2, 1.5, and 2.0, respectively. SRSs generated via this technique are assumed to give an upper bound on the response of an oscillator, with 5% to 10% of critical damping, located near the center of a buried facility. Approximate SRSs generated via this approach are assumed to represent the upper bound of the actual SRSs, independent of the precise form of the input motion.

Fragility Spectrum of Ideal Equipment

To illustrate the limitations of using an SRS for fragility assessment, a cantilever beam carrying a tip mass having both translational and rotary inertia was used as “ideal” equipment and was

FIG. 5 Cantilever beam carrying a tip mass with translational and rotary inertia.



subjected to a series of simulated shock tests. The equipment response was assumed to be linearly elastic. The mass density, cross-sectional area, Young's modulus, moment of inertia, and length of the beam are denoted by ρ , A , E , I , and L , respectively. These parameters were assumed constant along the beam. The mass and the radius of gyration of the tip mass are denoted by m and r , respectively. This simple equipment mass model is shown in **Fig. 5**. Exact solutions of the structural response $u(x, t)$ can be obtained via modal analysis if the support motion can be expressed in terms of a simple analytical function.

The equation of motion and the initial and boundary conditions for this structural system subjected to a support motion are derived herein. The support motion is prescribed as an acceleration time-history $\ddot{u}_g(t)$. The relative displacement of the beam with respect to the support is denoted by $u(x, t)$. From **Fig. 5**, the total beam deflection is

$$(1) \quad y(x, t) = u(x, t) + u_g(t)$$

where:

$u(x, t)$ = beam deflection with respect to the support, and
 $u_g(t)$ = support movement.

GOVERNING EQUATION

The transverse vibration problem of elastic beams has been investigated extensively in numerous textbooks with different boundary and initial conditions. Equations 2 through 12

essentially follow results presented in Refs 26, 27 through 28. The equation of motion for a differential beam element is

$$(2) \quad -\frac{\partial V}{\partial x} dx = \rho A dx \frac{\partial^2 y}{\partial t^2} = \rho A dx \frac{\partial^2}{\partial t^2} (u + u_g)$$

The shear force in the beam V is usually expressed as the moment gradient.

$$(3) \quad V = \frac{\partial M}{\partial x}$$

The beam moment-curvature relation is

$$(4) \quad M = EI \frac{\partial^2 u}{\partial x^2}$$

Substituting Eqs 3 and 4 into Eq 2 yields

$$(5) \quad -EI \frac{\partial^4 u}{\partial x^4} = \rho A \frac{\partial^2 u_g}{\partial t^2} + \rho A \frac{\partial^2 u}{\partial t^2}$$

or, alternatively,

$$(6) \quad \frac{\partial^4 u}{\partial x^4} + \frac{\rho A}{EI} \frac{\partial^2 u}{\partial t^2} = -\frac{\rho A}{EI} \frac{\partial^2 u_g}{\partial t^2}$$

The initial conditions are assumed to be at rest.

$$(7) \quad y(x, 0) = 0 \quad (0 \leq x \leq L)$$

$$(8) \quad \frac{\partial y}{\partial t}(x, 0) = 0 \quad (0 \leq x \leq L)$$

The boundary conditions at the fixed end are

$$(9) \quad u(0, t) = 0 \quad (t \geq 0)$$

$$(10) \quad \frac{\partial u}{\partial x}(0, t) = 0 \quad (t \geq 0)$$

The boundary conditions at the end attached to the tip mass are

$$(11) \quad EI \frac{\partial^2 u}{\partial x^2}(L, t) = -mr^2 \frac{\partial^2}{\partial t^2} \left[\frac{\partial u}{\partial x}(L, t) \right] \quad (t \geq 0)$$

$$(12) \quad EI \frac{\partial^3 u}{\partial x^3} = m \frac{\partial^2 y}{\partial t^2}(L, t) \quad (t \geq 0)$$

where Eqs 11 and 12 represent the moment and shear equilibrium conditions at the tip mass, respectively. The solution to the governing equations obtained via the method of separation of variables is also well known, namely, Eqs 13 through 47, except that the author converted the equations into a non-dimensional form (e.g., Eqs 13 through 15).

CLOSED-FORM SOLUTION

$$(13) \quad \text{Let } \alpha = \frac{u}{L}$$

$$(14) \quad \beta = \frac{u_g}{L}$$

$$(15) \quad \xi = \frac{x}{L}$$

Equation 6 can be rewritten as

$$(16) \quad \frac{\partial^4 \alpha}{\partial \xi^4} + \frac{\rho AL^4}{EI} \frac{\partial^2 \alpha}{\partial t^2} = \frac{\rho AL^4}{EI} \frac{\partial^2 \beta}{\partial t^2}$$

in which the negative sign of the support motion is dropped.

Introduce

$$(17) \quad T = L^2 \sqrt{\frac{\rho A}{EI}}$$

$$(18) \quad \psi = \frac{t}{T}$$

Equation 16 can be written in the dimensionless form

$$(19) \quad \frac{\partial^4 \alpha}{\partial \xi^4} + \frac{\partial^2 \alpha}{\partial \psi^2} = \frac{\partial^2 \beta}{\partial \psi^2}$$

with the corresponding initial and boundary conditions

$$(20) \quad \alpha(\xi, 0) = 0 \quad (0 \leq \xi \leq 1)$$

$$(21) \quad \frac{\partial \alpha}{\partial \psi}(\xi, 0) = 0 \quad (0 \leq \xi \leq 1)$$

$$(22) \quad \alpha(0, \psi) = 0 \quad (\psi \geq 0)$$

$$(23) \quad \frac{\partial \alpha}{\partial \xi}(0, \psi) = 0 \quad (\psi \geq 0)$$

$$(24) \quad \frac{\partial^2 \alpha}{\partial \xi^2}(1, \psi) = -\frac{mr^2}{\rho AL^3} \left[\frac{\partial^3 \alpha}{\partial \xi \partial \psi^2}(1, \psi) \right] \quad (\psi \geq 0)$$

$$(25) \quad \frac{\partial^3 \alpha}{\partial \xi^3}(1, \psi) = \frac{m}{\rho AL} \left[\frac{\partial^2 \alpha}{\partial \psi^2}(1, \psi) + \frac{\partial^2 \beta}{\partial \psi^2}(\psi) \right] \quad (\psi \geq 0)$$

The natural frequencies and mode shapes can be obtained from the homogeneous part of Eq 19.

$$(26) \quad \frac{\partial^4 \alpha}{\partial \xi^4} + \frac{\partial^2 \alpha}{\partial \psi^2} = 0$$

Solving it via the method of separation of variables,

$$(27) \quad \alpha(\xi, \psi) = \phi(\xi)\theta(\psi)$$

and using

$$(28) \quad \phi' = \frac{d\phi}{d\xi} \quad \text{and} \quad \dot{\theta} = \frac{d\theta}{d\psi}$$

Eq. 26 can be written as

$$(29) \quad \frac{\phi^{IV}}{\phi} + \frac{\ddot{\theta}}{\theta} = 0$$

and both terms must be constants; that is,

$$(30) \quad \frac{\phi^{IV}}{\phi} = -\frac{\ddot{\theta}}{\theta} = \lambda^4$$

The solution of ϕ takes the following form:

$$(31) \quad \phi = Af_1 + Bf_2 + Cf_3 + Df_4$$

where:

$$(32) \quad f_1 = \cosh \lambda \xi + \cos \lambda \xi$$

$$(33) \quad f_2 = \sinh \lambda \xi - \sin \lambda \xi$$

$$(34) \quad f_3 = \cosh \lambda \xi - \cos \lambda \xi$$

$$(35) \quad f_4 = \sinh \lambda \xi + \sin \lambda \xi$$

Given that $f_1(0) = 2$ and $f_2(0) = f_3(0) = f_4(0) = 0$, Eqs 22 and 31 yield $\phi(0) = 2A = 0$, and Eqs 23 and 28 yield $\phi'(0) = 2\lambda D = 0$. Therefore, $A = D = 0$.

Let

$$(36) \quad f_i(1) = F_i \quad i = 1, 2, 3, 4$$

$$(37) \quad \frac{m}{\rho AL} = k_1$$

$$(38) \quad \left(\frac{r}{L}\right)^2 = k_2$$

Then Eqs 24, 28, and 31 yield

$$(39) \quad \phi''(1)\theta = -k_1 k_2 \phi'(1)\ddot{\theta}$$

or

$$(40) \quad B(F_4 - k_1 k_2 \lambda^3 F_3) + C(F_1 - k_1 k_2 \lambda^3 F_4) = 0$$

and Eqs 25, 28, and 31 yield

$$(41) \quad \phi'''(1)\theta = k_1 \phi(1)\ddot{\theta}$$

or

$$(42) \quad B(F_1 + k_1 \lambda F_2) + C(F_2 + k_1 \lambda F_3) = 0$$

Equations 40 and 42 give relative values of B and C.

$$(43) \quad \frac{C}{B} = -\frac{F_4 - k_1 k_2 \lambda^3 F_3}{F_1 - k_1 k_2 \lambda^3 F_4} = -\frac{F_1 + k_1 \lambda F_2}{F_2 + k_1 \lambda F_3} = \gamma$$

A “characteristic equation” can be written as

$$(44) \quad (F_2 + k_1 \lambda F_3)(F_4 - k_1 k_2 \lambda^3 F_3) - (F_1 + k_1 \lambda F_2)(F_1 - k_1 k_2 \lambda^3 F_4) = 0$$

and each root of Eq 44, λ_i , is called a “characteristic value.”

For each λ_i , there is a corresponding ratio, given by Eq 43,

$$(45) \quad \gamma_i = \frac{C_i}{B_i}$$

which is used to determine the relative coefficients in the i th mode shape given by Eq 31.

From Eqs 16 and 30, it can be found that the solution of θ yields the natural circular frequencies ω_n , which are related to the characteristic values λ_n by

$$(46) \quad \omega_n^2 = \frac{\lambda_n^4 EI}{\rho AL^4}$$

and the natural cyclic frequencies can be expressed as

$$(47) \quad f_n = \frac{\lambda_n^2}{2\pi T}$$

in which n denotes the mode number.

If the structural response under support motion is linearly elastic, the total beam deflection $y(x,t)$ can be expressed as the sum of modal contributions.

MODAL EQUATIONS OF MOTION BY HAMILTON'S PRINCIPLE

Because of the orthogonality of vibration modes, each modal equation of motion can be solved separately as that for an SDOF system. Based on the principle of linear superposition, the total response of the system can be expressed as the sum of modal contributions. Equations 48 through 76 are the contribution of the author. The beam deflection $u(x,t)$ can be expressed in terms of relative modal amplitudes q_i and shapes η_i as

$$(48) \quad u(x, t) = \sum_{i=1}^{\infty} q_i(t) \eta_i(x)$$

and then

$$(49) \quad y(x, t) = \sum_{i=1}^{\infty} q_i(t) \eta_i(x) + u_g(t)$$

The kinetic energy of the system is

$$(50) \quad \Omega = \frac{1}{2} \int_0^L \rho A \left(\frac{\partial y}{\partial t} \right)^2 dx + \frac{1}{2} m \left(\frac{\partial y}{\partial t} \right)_{x=L}^2 + \frac{1}{2} m r^2 \left(\frac{\partial^2 y}{\partial x \partial t} \right)_{x=L}^2$$

and the strain energy of the system is

$$(51) \quad U = \frac{1}{2} \int_0^L EI \left(\frac{\partial^2 u}{\partial x^2} \right)^2 dx$$

Applying Hamilton's principle,

$$(52) \quad \int_{t_1}^{t_2} \delta(\Omega - U) dt = 0$$

where

$$(53) \quad \delta\Omega = \int_0^L \rho A \dot{y} \delta \dot{y} dx + m \dot{y}_L \delta \dot{y}_L + m r^2 \dot{u}'_L \delta \dot{u}'_L$$

$$(54) \quad \delta U = \int_0^L EI u'' \delta u'' dx$$

Using the expressions

$$(55) \quad \dot{y} = \sum_{i=1}^{\infty} \dot{q}_i \eta_i + \dot{u}_g$$

$$(56) \quad \delta \dot{y} = \delta \dot{u} = \sum_{i=1}^{\infty} \delta \dot{q}_i \eta_i$$

$$(57) \quad \dot{y}_L = \dot{u}_L + \dot{u}_g = \sum_{i=1}^{\infty} \dot{q}_i \eta_i(L) + \dot{u}_g$$

$$(58) \quad \delta \dot{y}_L = \delta \dot{u}_L = \sum_{i=1}^{\infty} \delta \dot{q}_i \eta_i(L)$$

$$(59) \quad u' = \sum_{i=1}^{\infty} q_i \eta'_i$$

$$(60) \quad \dot{u}' = \sum_{i=1}^{\infty} \dot{q}_i \eta'_i$$

$$(61) \quad \dot{u}'_L = \sum_{i=1}^{\infty} \dot{q}_i \eta'_i(L)$$

$$(62) \quad \delta \dot{u}'_L = \sum_{i=1}^{\infty} \delta \dot{q}_i \eta'_i(L)$$

$$(63) \quad u'' = \sum_{i=1}^{\infty} q_i \eta''_i$$

$$(64) \quad \delta u'' = \sum_{i=1}^{\infty} \delta q_i \eta''_i$$

Eq. 52 can be written as

$$(65) \quad \int_{t_1}^{t_2} \left[\int_0^L \rho A \left(\sum \dot{q}_i \eta_i + \dot{u}_g \right) \left(\sum \delta \dot{q}_i \eta_i \right) dx + m \left(\sum \dot{q}_i \eta_i(L) + \dot{u}_g \right) \left(\sum \delta \dot{q}_i \eta_i(L) \right) + m r^2 \left(\sum \dot{q}_i \eta'_i(L) \right) \left(\sum \delta \dot{q}_i \eta'_i(L) \right) - \int_0^L EI \left(\sum q_i \eta''_i \right) \left(\sum \delta q_i \eta''_i \right) dx \right] dt = 0$$

$$(66) \quad \int_0^L \rho A \left(\sum \dot{q}_i \eta_i + \dot{u}_g \right) \left(\sum \delta \dot{q}_i \eta_i \right) dx = \sum_{i=1}^{\infty} \sum_{j=1}^{\infty} \dot{q}_i \delta \dot{q}_j \int_0^L \rho A \eta_i \eta_j dx + \dot{u}_g \sum_{i=1}^{\infty} \delta \dot{q}_i \int_0^L \rho A \eta_i dx$$

$$\begin{aligned}
& m \left(\sum \dot{q}\eta(L) + \dot{u}_g \right) \left(\sum \delta \dot{q}\eta(L) \right) \\
(67) \quad & = m \sum_{i=1}^{\infty} \sum_{j=1}^{\infty} \dot{q}_i \delta \dot{q}_j \eta_i(L) \eta_j(L) + m \dot{u}_g \sum_{i=1}^{\infty} \delta \dot{q}_i \eta_i(L)
\end{aligned}$$

$$(68) \quad m r^2 \left(\sum \dot{q}\eta'(L) \right) \left(\sum \delta \dot{q}\eta'(L) \right) = m r^2 \sum_{i=1}^{\infty} \sum_{j=1}^{\infty} \dot{q}_i \delta \dot{q}_j \eta'_i(L) \eta'_j(L)$$

$$(69) \quad \int_0^L EI \left(\sum q\eta'' \right) \left(\sum \delta q\eta'' \right) dx = \sum_{i=1}^{\infty} \sum_{j=1}^{\infty} q_i \delta q_j \int_0^L EI \eta'_i \eta'_j dx$$

Integrating Eq 65 by parts and using Eqs 66 through 69,

$$\begin{aligned}
& \sum_{i=1}^{\infty} \sum_{j=1}^{\infty} \left(\int_0^L \rho A \eta_i \eta_j dx \dot{q}_i \delta q_j \Big|_{t_1}^{t_2} - \int_{t_1}^{t_2} \ddot{q}_i \delta q_j \int_0^L \rho A \eta_i \eta_j dx dt \right) \\
& + \sum_{i=1}^{\infty} \left(\dot{u}_g \int_0^L \rho A \eta_i dx \delta q_i \Big|_{t_1}^{t_2} - \int_{t_1}^{t_2} \ddot{u}_g \delta q_i \int_0^L \rho A \eta_i dx dt \right) \\
& + m \sum_{i=1}^{\infty} \sum_{j=1}^{\infty} \left(\eta_i(L) \eta_j(L) \dot{q}_i \delta q_j \Big|_{t_1}^{t_2} - \int_{t_1}^{t_2} \ddot{q}_i \delta q_j \eta_i(L) \eta_j(L) dt \right) \\
& + m \sum_{i=1}^{\infty} \left(\dot{u}_g \eta_i(L) \delta q_i \Big|_{t_1}^{t_2} - \int_{t_1}^{t_2} \ddot{u}_g \delta q_i \eta_i(L) dt \right) \\
& + m r^2 \sum_{i=1}^{\infty} \sum_{j=1}^{\infty} \left(\eta'_i(L) \eta'_j(L) \dot{q}_i \delta q_j \Big|_{t_1}^{t_2} - \int_{t_1}^{t_2} \ddot{q}_i \delta q_j \eta'_i(L) \eta'_j(L) dt \right) \\
& - \sum_{i=1}^{\infty} \sum_{j=1}^{\infty} q_i \delta q_j \int_0^L EI \eta'_i \eta'_j dx = 0
\end{aligned}$$

(70)

Rearranging terms yields

$$\begin{aligned}
& \sum_{i=1}^{\infty} \sum_{j=1}^{\infty} \int_{t_1}^{t_2} \left\{ \ddot{q}_i \left[\int_0^L \rho A \eta_i \eta_j dx + m \eta_i(L) \eta_j(L) + m r^2 \eta'_i(L) \eta'_j(L) \right] \right. \\
& \quad \left. + q_i \int_0^L EI \eta'_i \eta'_j dx \right\} \delta q_j dt \\
& = - \sum_{i=1}^{\infty} \int_{t_1}^{t_2} \ddot{u}_g \left[\int_0^L \rho A \eta_i dx + m \eta_i(L) \right] \delta q_i dt
\end{aligned}$$

(71)

It can be shown based on the orthogonality of mode shapes that

$$(72) \quad \int_0^L \rho A \eta_i \eta_j dx + m \eta_i(L) \eta_j(L) + m r^2 \eta'_i(L) \eta'_j(L) = \bar{\delta}_{ij}$$

where $\bar{\delta}_{ij} = 1$ if $i = j$ and $\bar{\delta}_{ij} = 0$ if $i \neq j$.

Furthermore,

$$\begin{aligned}
& \int_0^L EI \eta'_i \eta'_j dx = 0 \quad \text{for } i \neq j \\
& = \frac{EI}{L^3} \lambda_i^4 \quad \text{for } i = j
\end{aligned}$$

(73)

Substituting Eqs 72 and 73 into Eq 71,

$$(74) \quad \int_{t_1}^{t_2} \sum_{i=1}^{\infty} \left(\ddot{q}_i + \frac{EI}{L^3} \lambda_i^4 q_i + \ddot{u}_g \left[\int_0^L \rho A \eta_i dx + m \eta_i(L) \right] \right) \delta q_i dt = 0$$

Because δq_i are arbitrary variations, it is necessary that

$$(75) \quad \ddot{q}_i + \frac{EI}{L^3} \lambda_i^4 q_i = -\ddot{u}_g \left[\int_0^L \rho A \eta_i dx + m \eta_i(L) \right]$$

for all values of i . Equation 75 is the equation of motion for mode i , and its non-dimensional form can be expressed as

$$(76) \quad \ddot{\theta}_i + \frac{\lambda_i^4}{T} \theta_i = -\ddot{\beta} \left[\int_0^1 \phi_i d\xi + k_1 \phi_i(1) \right]$$

in which the sum of the terms in the bracket is the “effective modal mass.”

Numerical Simulation of Fragility Experiment

The shock response of a hypothetical piece of equipment is assumed to be “perfectly” represented by the cantilever beam with a tip mass model. The parameters of the model are given in **Table 1**. Based on Eqs 17, 37, and 38, the characteristic period of the system, $T = 0.02$ s, along with $k_1 = 1$ and $k_2 = 0.0025$, is used for this example. The characteristic curve (i.e., the plot of Eq 44) of this system is shown in **Fig. 6**. The roots of this curve are the characteristic values of the free-vibration equation (Eq 26), and the corresponding characteristic functions (obtained from Eqs 31 and 43) are the free-vibration mode shapes. Although there are infinite numbers of natural vibration modes existing in this system, only the first seven modes are retained for a modal analysis. The characteristic values of these modes are identified in **Fig. 6**, and the associated modal properties are given in **Table 2**. The normalized shapes of the first seven modes are shown in **Fig. 7**. The accuracy of the characteristic values and mode shapes deteriorates with higher modes,

TABLE 1 Parameters of a cantilever beam with a tip mass model.

Model Parameter	Value
Length L , in.	36
Cross-sectional area A , in. ²	10
Mass density ρ , lb/ft ³	12.5
Tip mass m , lb	2.6
Radius of gyration r , in.	1.8
Young's modulus E , psi	4 000 000
Moment of inertia I , in. ⁴	2.36

FIG. 6

Characteristic curve.

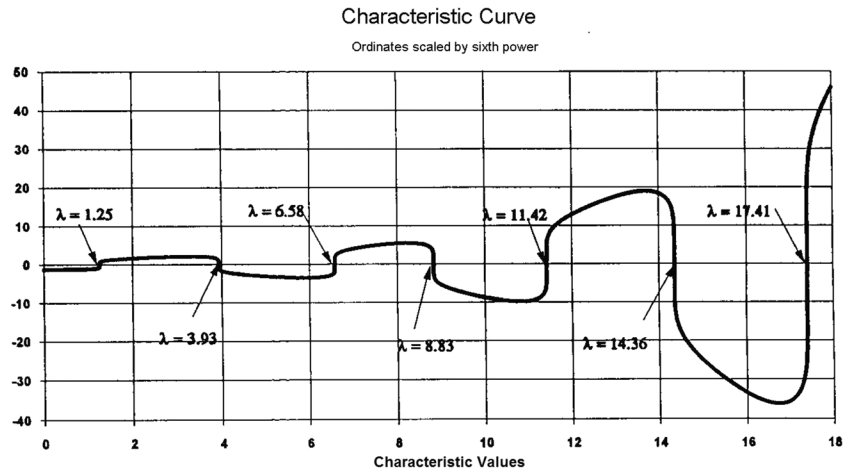


TABLE 2 Modal properties.

Mode Number	Characteristic Value	Cyclic Frequency f_n , Hz	Effective Mass
1	1.247	12.37	0.976
2	3.928	122.78	0.471
3	6.577	344.23	0.254
4	8.832	620.74	0.186
5	11.417	1037.28	0.162
6	14.355	1639.82	0.135
7	17.414	2413.17	0.057

but the contributions from higher modes are relatively insignificant.

The base acceleration expression can be derived from Eq 14 as

$$(77) \quad \ddot{u}_g(t) = \frac{d^2 u_g}{dt^2} = \frac{L}{T^2} \ddot{\beta}(\psi)$$

A unit triangular pulse with duration t_d and no rise time was used to simulate the support motion (or base acceleration) caused by an explosion. Mathematically, the base acceleration can be expressed as

$$(78) \quad \ddot{\beta}(\psi) = 1 - \frac{\psi}{\left(\frac{t_d}{T}\right)}$$

$$(79) \quad \text{Let } a^2 = \frac{\lambda^4}{T} \quad \text{and} \quad K = \int_0^1 \phi_i d\xi + k_1 \phi_i(1)$$

The exact solution to Eq 76 can be expressed as

FIG. 7

Mode shapes of the cantilever beam with a tip mass.

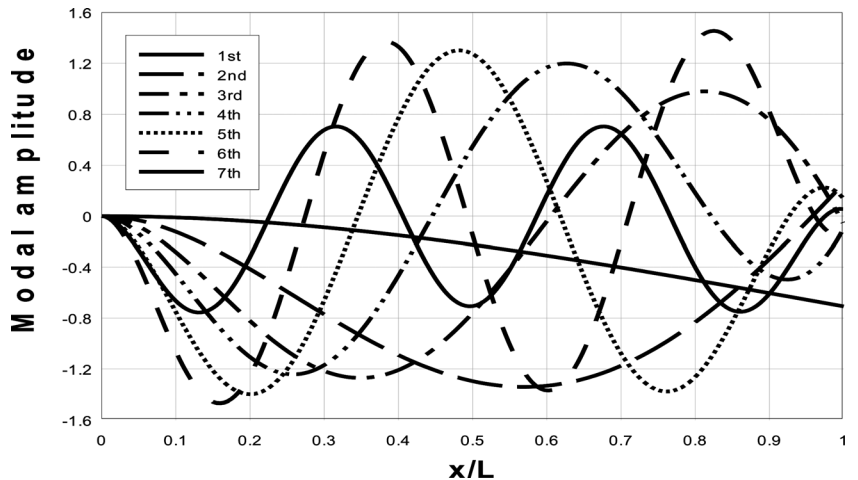
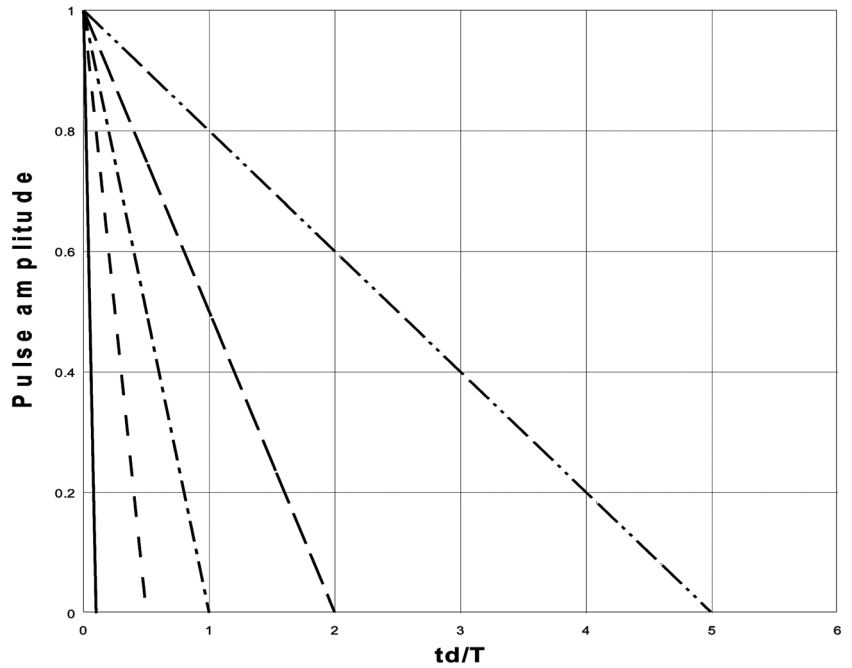


FIG. 8

Base acceleration pulses.



$$\theta(\psi) = \frac{K}{a^2} \cos(a\psi) - \frac{K}{a^3 \left(\frac{t_d}{T}\right)} \sin(a\psi) - \frac{K}{a^2} \left(1 - \frac{\psi}{\left(\frac{t_d}{T}\right)}\right)$$

(80) $0 \leq \psi \leq \frac{t_d}{T}$

Free vibration ensues at the end of the triangular pulse. In the example, the pulse duration is varied as $t_d/T = 0.1, 0.5, 1, 2,$ and 5 , as shown in **Fig. 8**. A frequency domain analysis of the time histories of pulses reveals that the shorter the pulse duration, the broader the frequency contents. However, the energy level is lower for shorter pulses. The equipment response is assumed to be represented accurately by the first seven modes, covering a response frequency range between 0 and 2500 Hz.

The effects of the pulse duration on the equipment response parameters, such as the tip mass displacement, base shear, and base moment, were evaluated for the various t_d/T . The multiple-degree-of-freedom (i.e., seven modes) shock responses are compared to the SDOF (i.e., first mode only) responses in **Table 3**. The differences are also given as percentages of error therein. There is no difference in the tip mass displacements; however, the maximum base shear and base moment of the multiple-degree-of-freedom responses will always exceed the responses of a simple oscillator. The errors introduced by ignoring the higher modes are as high as 43 % in base shear and 14 % in base moment. Note that the shorter the shock duration, the greater the error. A typical time history of the base shear and the corresponding Fourier spectrum are

shown in **Figs. 9(a)** and **9(b)**, respectively. The spectrum shows significant responses at 85, 870, and 2435 Hz, even though responses from lower modes are also present. A typical time history of the base moment and the corresponding power density spectrum are shown in **Figs. 10(a)** and **10(b)**, respectively. Although there is power spectral density at the fundamental frequency of 12 Hz, most of the structural response is associated with 85 Hz. There is also a minor response at 870 Hz. Equipment failure may be related to peak displacement, shear, moment, or strains at given locations on a component. The base acceleration pulse amplitude can be adjusted until a failure occurs. The fragility spectrum can subsequently be established. The fragility spectrum thus depends upon the base acceleration pulse duration.

It is common practice to use the fundamental frequency of a multiple-degree-of-freedom system and enter the “design” SRS for a given support motion to determine the peak structural response of the system. The contributions from higher modes are generally ignored. Let us assume the beam in the above example would fail under a base shear of 50 lb. If the SDOF beam were subjected to a peak base acceleration triangular pulse of 230 g with a 2-ms duration, the “design” SRS (see **Fig. 1**) would show a peak response at a frequency of 12.37 Hz. The maximum base shear and base moment induced would be 31 lb and 87 ft lb, respectively. Had the “real” beam been subjected to shaker table testing, the fragility spectrum would have shown peak responses at frequencies of 12, 85, 870, and 2435 Hz. The maximum base shear and base moment induced would have

TABLE 3 Effect of pulse duration on structural response.

t_d/T	Tip Displacement, in.		Base Shear, lb			Base Moment, ft lb		
	Seven Modes	First Mode	Seven Modes	First Mode	Percent Difference	Seven Modes	First Mode	Percent Difference
0.1	0.11	0.11	54	31	43	101	87	14
0.5	0.31	0.31	120	88	27	264	245	7
1	0.36	0.36	140	102	27	305	283	7
2	0.38	0.38	149	109	27	325	305	6
5	0.40	0.40	152	114	25	338	318	6

been 54 lb and 101 ft lb, respectively. So, the SDOF model would indicate no failure, whereas the real beam would have failed in the shaker table test. Thus, assuming that the total response of the equipment is predominantly in the first mode can lead to significant error.

Conclusions

This study points out the shortcomings of the SRS approach to characterizing equipment shock fragility.

- (1) SRS-based fragility spectra are not unique. Even for equipment that can be modeled closely by a simple spring-mass oscillator, different base excitations generally produce different fragility spectra.

- (2) Assuming the total response of an equipment is predominantly in the first mode can lead to significant error. In order to rigorously quantify the errors due to ignoring responses from higher modes, the exact solution to the transverse vibration problem of a cantilever beam with a tip mass having rotary inertia was presented in the shock response analyses.

In conclusion, this study has revealed the inadequacy of the SRS for characterizing the shock fragility of equipment. A more rigorous analytical approach for assessing equipment fragility is needed.

FIG. 9 (a) Base shear time history for $t_d/T = 0.5$. (b) Fourier spectrum of base shear time history for $t_d/T = 0.5$.

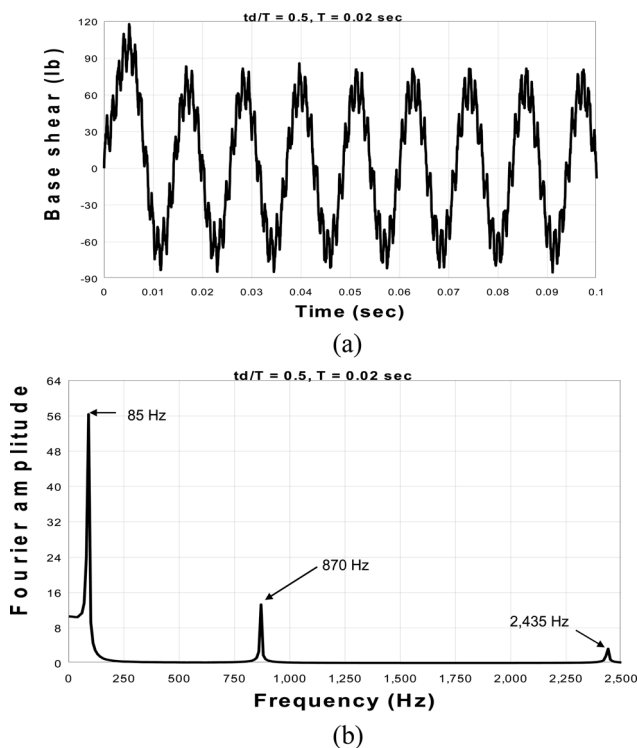
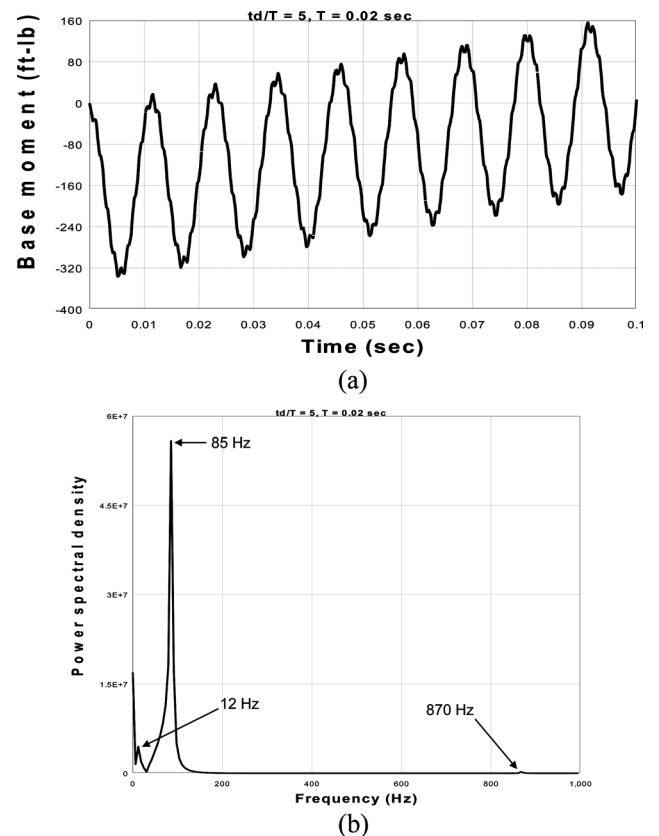


FIG. 10 (a) Base moment time history for $t_d/T = 5$. (b) Power spectrum of base moment time history for $t_d/T = 5$.



References

- [1] Pan, Y., Agrawal, A. K., and Ghosn, M., "Seismic Fragility of Continuous Steel Highway Bridges in New York State," *J. Bridge Eng.*, Vol. 12(6), 2007, pp. 689–699.
- [2] Zhong, J. S., Gardoni, P., Rosowsky, D., and Haukaas, T., "Probabilistic Seismic Demand Models and Fragility Estimates for Reinforced Concrete Bridges With Two-Column Bents," *J. Eng. Mech.*, Vol. 134(6), 2008, pp. 495–504.
- [3] Liang, C.-C., Yang, M.-F., and Tai, Y.-S., "Prediction of Shock Response for a Quadropod- mast Using Response Spectrum Analysis Method," *Ocean Eng.*, Vol. 29(8), 2002, pp. 887–914.
- [4] Shattarat, N. K., Symans, M. D., McLean, D. I., and Cofer, W. F., "Evaluation of Nonlinear Static Analysis Methods and Software Tools for Seismic Analysis of Highway Bridges," *Eng. Struct.*, Vol. 30(5), 2008, pp. 1335–1345.
- [5] Nielson, B. G. and DesRoches, R., "Seismic Fragility Methodology for Highway Bridges," *Structural Engineering and Public Safety: Proceedings of the 2006 Structures Congress*, St. Louis, MO, May 18–21, 2006, American Society of Civil Engineers (ASCE), pp. 1–9.
- [6] Yang, C. S., DesRoches, R., and Padgett, J. E., "Analytical Fragility Models for Box Girder Bridges With and Without Protective Systems," *Proceedings of the 2009 Structures Congress*, Austin, TX, April 30–May 2, 2009, American Society of Civil Engineers (ASCE).
- [7] Kim, S. H. and Shinozuka, M., "Fragility Curves for Concrete Bridges Retrofitted by Column Jacketing and Restrainers," *Proceedings of 6th U.S. Conference and Workshop on Lifeline Earthquake Engineering*, Long Beach, CA, Aug 10–13, 2003, American Society of Civil Engineers (ASCE).
- [8] Porter, K., Hamburger, R., and Kennedy, R., "Practical Development and Application of Fragility Functions," *Proceedings of the 2007 Structures Congress*, Long Beach, CA, May 16–19, 2007, American Society of Civil Engineers (ASCE).
- [9] Zhang, J. and Huo, Y., "Fragility Function of Base Isolated Highway Bridges," *Proceedings of 18th Analysis and Computation Specialty Conference*, Vancouver, BC, Canada, April 24–26, 2008, American Society of Civil Engineers (ASCE), pp. 1–17.
- [10] Chaudhuri, S. R. and Hutchinson, T. C., "Fragility of Bench-Mounted Equipment Considering Uncertain Parameters," *J. Struct. Eng.*, Vol. 132(6), 2006, pp. 884–898.
- [11] Wilcoski, J., Gambill, J. B., and Smith, S. J., "The CERL Equipment Fragility and Protection Procedure (CEFAPP): Experimental Definition of Equipment Vulnerability to Transient Support Motions," *USACERL Technical Report No. 97/58*, U.S. Army Corps of Engineers Construction Engineering Research Laboratories, Champaign, IL 1997.
- [12] Dastous, J.-B. and Filiatrault, A., "Seismic Displacement at Interconnection Points of Substation Equipment," *Proceedings of 6th U.S. Conference and Workshop on Lifeline Earthquake Engineering*, Long Beach, CA, Aug 10–13, 2003, American Society of Civil Engineers (ASCE).
- [13] Straub, D. and Der Kiureghian, A., "Improved Seismic Fragility Modeling From Empirical Data," *Struct. Safety*, Vol. 30(4), 2008, pp. 320–336.
- [14] Zhu, Z. Y. and Soong, T. T., "Toppling Fragility of Unrestrained Equipment," *Earthquake Spectra*, Vol. 14(4), 1998, pp. 695–712.
- [15] Safford, F. B. and Tuttle, R. J., "Transient Shock Fragility and Hardness Assessment of Commercial Communications Equipment," *Document No. 740801*, SAE International, Warrendale, PA, 1974.
- [16] Cunniff, P. F. and O'Hara, G. J., "A Procedure for Generating Shock Design Values," *J. Sound Vib.*, Vol. 134(1), 1989, pp. 155–164.
- [17] Salmonte, A. J., "Evaluation of Secondary and Higher Order Response Facets in Response Spectrum Analysis," *Nucl. Eng. Des.*, Vol. 109(3), 1988, pp. 433–454.
- [18] Merkle, D. H., Rochefort, M. A., and Tuan, C. Y., "Equipment Shock Tolerance," *Final Report ESL-TR-92-65*, U.S. Air Force Civil Engineering Support Agency, Tyndall Air Force Base, FL, 1993.
- [19] MIL-STD-202G, U.S. Department of Defense, Test Method Standard, Electronic and Electrical Component Parts, February 2002, 191p.
- [20] ISO 16750-3, International Standards Organization, International Standard, Road Vehicles — Environmental Conditions and Testing for Electrical and Electronic Equipment, Part 3: Mechanical Loads, December 2003, 34p.
- [21] SAE J1455, SAE International, Recommended Environmental Practices for Electronic Equipment Design in Heavy-Duty Vehicle Applications, August, 2012.
- [22] U.S. Army, "Pyrotechnic Shock Test Procedure: Test Operations Procedure 5-2-521," Final Report, U.S. Army Developmental Test Command, Aberdeen Proving Ground, MD, 2007.
- [23] MIL-STD-810G, U. S. Department of Defense, Test Method Standard, Environmental Engineering Considerations and Laboratory Tests, October 2008, 804 p.
- [24] Coomes, J. R. and Roberts, W. B., "Report of Test on BUZZER, TYPE A-3 Submitted by Navy Yard, Portsmouth, N.H.," *Report No. NRL-1396*, Naval Research Laboratory, Washington, D.C., 1937.
- [25] Kiger, S. A., Balsara, J. P., and Baylot, J. T., "A Computational Procedure for Peak In-structure Motions and Shock Spectra for Conventional Weapons," *Shock and Vibration Bulletin*, No. 54, Part 2, 1984, pp. 223–226.
- [26] Clough, R. W. and Penzien, J., *Dynamics of Structures*, McGraw-Hill, New York, 1975.
- [27] Craig, R. R., *Structural Dynamics—An Introduction to Computer Methods*, Wiley, New York, 1981, pp. 192–204.
- [28] Meirovitch, L., *Elements of Vibration Analysis*, McGraw-Hill, New York, 1986, pp. 220–232.